



# Highly Tunable Emission by Halide Engineering in Lead-Free Perovskite-Derivative Nanocrystals: The Cs<sub>2</sub>SnX<sub>6</sub> (X = Cl, Br, Br/I, I) System

Alessandro Veronese<sup>1</sup>, Maddalena Patrini<sup>1\*</sup>, Daniele Bajoni<sup>2</sup>, Carlo Ciarrocchi<sup>3</sup>, Paolo Quadrelli<sup>3</sup> and Lorenzo Malavasi<sup>3\*</sup>

<sup>1</sup> Department of Physics and CNISM, University of Pavia, Pavia, Italy, <sup>2</sup> Department of Electrical, Computer and Biomedical Engineering, University of Pavia, Pavia, Italy, <sup>3</sup> Department of Chemistry and INSTM, University of Pavia, Pavia, Italy

## OPEN ACCESS

### Edited by:

Silvia Colella,  
University of Salento, Italy

### Reviewed by:

Zhiguo Xia,  
University of Science and Technology  
Beijing, China  
Elisabetta Fanizza,  
University of Bari Aldo Moro, Italy

### \*Correspondence:

Maddalena Patrini  
maddalena.patrini@unipv.it  
Lorenzo Malavasi  
lorenzo.malavasi@unipv.it

### Specialty section:

This article was submitted to  
Inorganic Chemistry,  
a section of the journal  
Frontiers in Chemistry

Received: 30 September 2019

Accepted: 13 January 2020

Published: 31 January 2020

### Citation:

Veronese A, Patrini M, Bajoni D, Ciarrocchi C, Quadrelli P and Malavasi L (2020) Highly Tunable Emission by Halide Engineering in Lead-Free Perovskite-Derivative Nanocrystals: The Cs<sub>2</sub>SnX<sub>6</sub> (X = Cl, Br, Br/I, I) System. *Front. Chem.* 8:35. doi: 10.3389/fchem.2020.00035

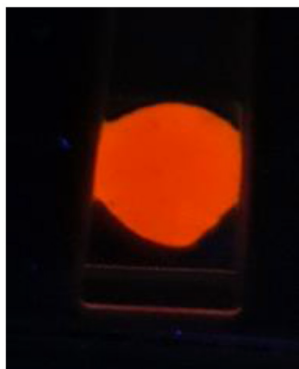
Nanocrystals of Cs<sub>2</sub>SnX<sub>6</sub> (X = Cl, Br, Br<sub>0.5</sub>I<sub>0.5</sub>, and I) have been prepared by a simple, optimized, hot-injection method, reporting for the first time the synthesis of Cs<sub>2</sub>SnCl<sub>6</sub>, Cs<sub>2</sub>SnBr<sub>6</sub>, and mixed Cs<sub>2</sub>Sn(I<sub>0.5</sub>Br<sub>0.5</sub>)<sub>6</sub> nanocrystalline samples. They all show a cubic crystal structure with a linear scaling of lattice parameter by changing the halide size. The prepared nanocrystals have spherical shape with average size from 3 to 6 nm depending on the nature of the halide and span an emission range from 444 nm (Cs<sub>2</sub>SnCl<sub>6</sub>) to 790 nm (Cs<sub>2</sub>SnI<sub>6</sub>) with a further modulation provided by mixed Br/I systems.

**Keywords:** spectroscopy, lead-free, emission, perovskite, nanocrystal, nanocrystal (NC)

## INTRODUCTION

The extremely facile synthesis and the impressive optical properties of metal halide perovskites (MHPs) nanocrystals (NCs) make them an ideal class of materials for several optoelectronic devices, with the possibility of replacing, in the future, other conventional semiconductors in everyday life applications (Amgar et al., 2016; Huang et al., 2016, 2017; Kovalenko et al., 2017; Swarnkar et al., 2017). The major issue of current metal halide perovskites, such as CsPbX<sub>3</sub> (X = Cl, Br, I), is the presence of lead, a toxic metal that raises a great concern in view of applications. While trying to overcome this issue, researchers are exploring new compounds that substitute lead with more environmental-friendly elements, e.g., tin, germanium, bismuth, palladium, or antimony (Jellicoe et al., 2016; Liu et al., 2017; Pal et al., 2017; Wang et al., 2017; Yang et al., 2017; Zhang et al., 2017; Bekenstein et al., 2018; Creutz et al., 2018; Leng et al., 2018; Sun et al., 2018; Wu et al., 2018; Zhou et al., 2018a,b). These alternative perovskites at the moment still present poorer optical properties as compared to lead-based ones. Nevertheless, they are of primary interest for the development of this research topic and they deserve more and deeper investigations, both theoretical and experimental, to improve their performances.

Tin halide perovskites represent a promising alternative to lead halide perovskites, especially for photovoltaic applications. Due to the higher electronegativity of tin, these compounds have indeed a narrower band-gap in comparison to their lead-containing counterparts, and so they are potentially better light harvesters (Mancini et al., 2015; Jellicoe et al., 2016; Ferrara et al., 2017; Pisanu et al., 2018). Tin-based perovskites, however, suffer from a severe chemical instability that



**GRAPHICAL ABSTRACT** | The series of  $\text{Cs}_2\text{SnX}_6$  ( $X = \text{Cl, Br, Br}_{0.5}\text{I}_{0.5}, \text{ and I}$ ) nanocrystals with average size around 3 nm is reported with the first synthesis of Br, and mixed Br/I compounds. A progressive tuning of structural and optical properties is observed along with the anion composition. The nanocrystals are stable for several days under ambient conditions.

heavily hampers the investigation of their physical properties. Under ambient conditions,  $\text{Sn}^{2+}$  tends to easily oxidize into the more stable  $\text{Sn}^{4+}$ ; the problem of oxidation is even more pronounced in the case of NCs because of the higher surface–volume ratio. This undesired transition is followed by the creation of trap states that irreversibly deteriorate the light emission properties of the crystals, thus suggesting a defect-intolerant nature of tin-based perovskites. Moreover, spin–orbit coupling of Sn  $5p$  states is weaker compared to that of Pb  $6p$  states, therefore their conduction band (CB) is less stabilized and the probability of formation of trap states is increased (Hermann et al., 2010; Umari et al., 2015).

A possible strategy to overcome this problem is to replace  $\text{Sn}^{2+}$  with  $\text{Sn}^{4+}$  in order to avoid its oxidation. This substitution modifies the standard perovskite crystal structure and leads to the formation of a so-called vacancy-ordered double perovskite. In this perovskite derivative, the B-sites are alternatively occupied by a tetravalent ion and vacancies, and the  $\text{BX}_6$  octahedra result thereby to be isolated (Cai et al., 2017; Dalpian et al., 2017; Ju et al., 2018). At present, studies on  $\text{Sn}^{4+}$ -based double perovskites in the form of colloidal nanocrystals are still very limited and only the synthesis of  $\text{Cs}_2\text{SnI}_6$  and, very recently, of Mn-doped  $\text{Cs}_2\text{SnCl}_6$  NCs was reported by few groups employing different synthetic procedures (Wang et al., 2016; Dolzhenkov et al., 2017; Ghosh et al., 2018; Jing et al., 2019; Lin et al., 2019; Xu et al., 2019). Wang et al. (2016) demonstrated an enhancement in the chemical stability of  $\text{Cs}_2\text{SnI}_6$  NCs compared to those based on  $\text{Sn}^{2+}$ . The synthesis and purification of the crystals were performed under ambient conditions and, after 1 week of storage out of glove-box, the samples did not show degradation of the optical properties.

The interest on these perovskite  $\text{Sn}^{4+}$  containing materials is then relevant for basic and applied research and it would be of great importance to extend their optical properties through stoichiometry manipulation such as anion substitution, as already performed in other NCs systems (Jellicoe et al., 2016). To the best of our knowledge, only  $\text{Cs}_2\text{SnI}_6$  NCs and  $\text{Cs}_2\text{SnCl}_6$  have been described in the current literature in the past, while

in the present paper we are reporting on the synthesis of the whole set of nanocrystalline  $\text{Cs}_2\text{SnX}_6$  materials with  $X = \text{Cl, Br, I, and mixed I/Br}$  achieved by means of an optimization of the currently reported synthesis methods for  $\text{Cs}_2\text{SnI}_6$  (Wang et al., 2016; Dolzhenkov et al., 2017; Ghosh et al., 2018; Xu et al., 2019). A clear and monotonic modulation of structural and optical properties with anion composition has been observed in the prepared  $\text{Cs}_2\text{SnX}_6$  NCs, similarly to 3D-perovskite analogs, with a significant variation of the band gap from 1.58 eV ( $\text{Cs}_2\text{SnI}_6$ ) to 3.86 eV ( $\text{Cs}_2\text{SnCl}_6$ ) and emission properties in line or even better with respect to available reports on  $\text{Cs}_2\text{SnI}_6$  (Wang et al., 2016; Dolzhenkov et al., 2017; Ghosh et al., 2018; Xu et al., 2019).

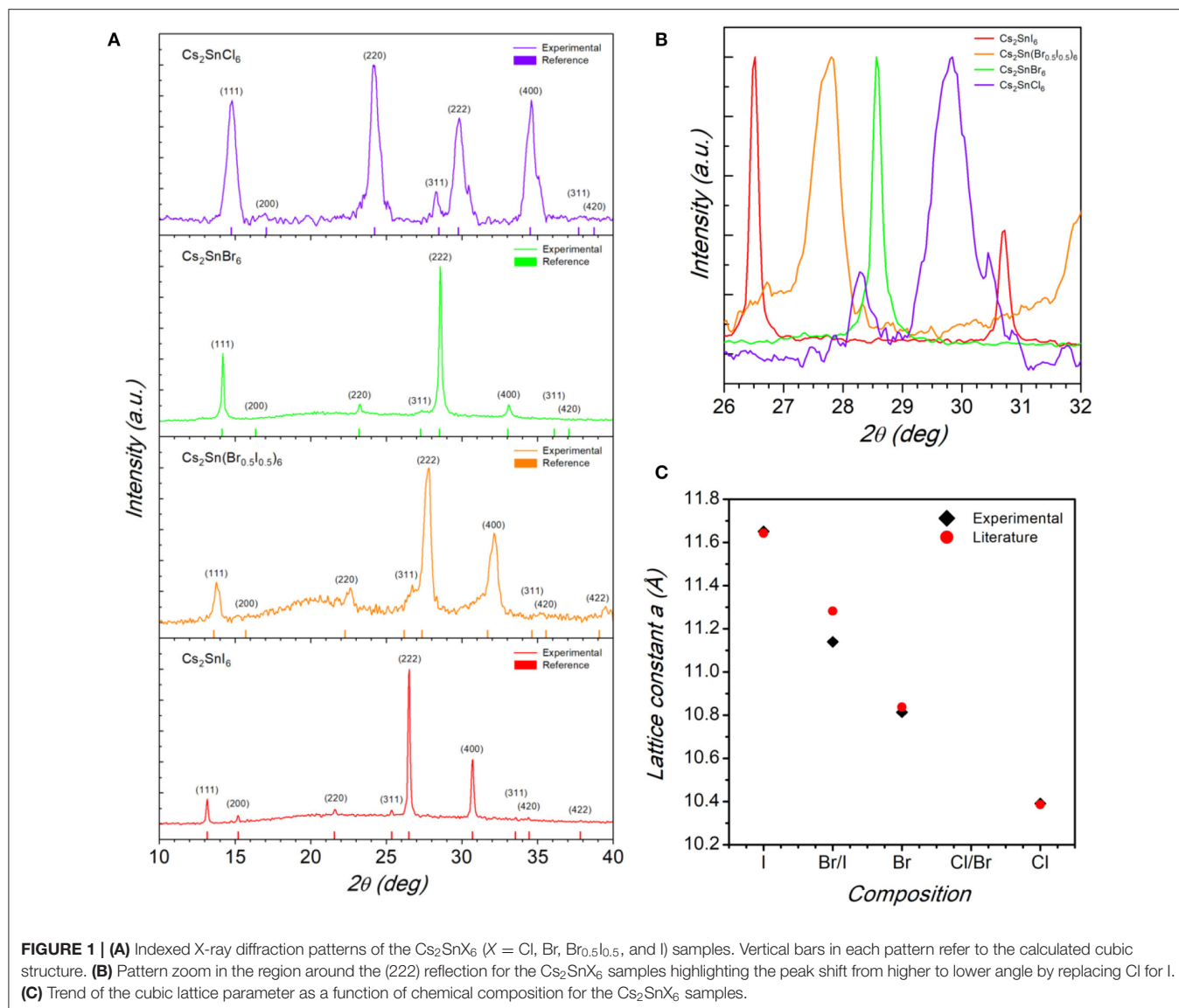
## RESULTS AND DISCUSSION

Nanocrystalline  $\text{Cs}_2\text{SnX}_6$  ( $X = \text{Cl, Br, Br}_{0.5}\text{I}_{0.5}, \text{ and I}$ ) samples have been synthesized according to the methodology reported in the Experimental Section through an optimized route with respect to the available ones (Jellicoe et al., 2016; Wang et al., 2016; Dolzhenkov et al., 2017; Ghosh et al., 2018; Xu et al., 2019). The laboratory powder X-ray diffraction (XRD) patterns of the  $\text{Cs}_2\text{SnX}_6$  ( $X = \text{Cl, Br, Br}_{0.5}\text{I}_{0.5}, \text{ and I}$ ) samples are reported in **Figure 1A**.

From the patterns reported in **Figure 1A** it is possible to note that all the sample are single-phase and can be indexed according to the cubic  $Fm\bar{3}m$  space group, as previously reported for  $\text{Cs}_2\text{SnI}_6$  and  $\text{Cs}_2\text{SnCl}_6$  (Wang et al., 2016; Dolzhenkov et al., 2017; Jing et al., 2019; Lin et al., 2019; Xu et al., 2019). By a simple visual inspection of the main reflection in **Figure 1B**, i.e., the (222), a shift to higher  $2\theta$  values passing from  $\text{Cs}_2\text{SnI}_6$  (bottom panel in **Figure 1A**) to  $\text{Cs}_2\text{SnCl}_6$  (top panel) is clear, indicating a reduction of the cubic cell size by replacing I with Cl. The trend of cubic lattice parameter determined for the four samples is reported in **Figure 1C**, showing a significant change of the unit cell from 11.642(2) Å for  $\text{Cs}_2\text{SnI}_6$  to 10.391(2) Å for  $\text{Cs}_2\text{SnCl}_6$  with a reasonable linear scaling as a function of composition.

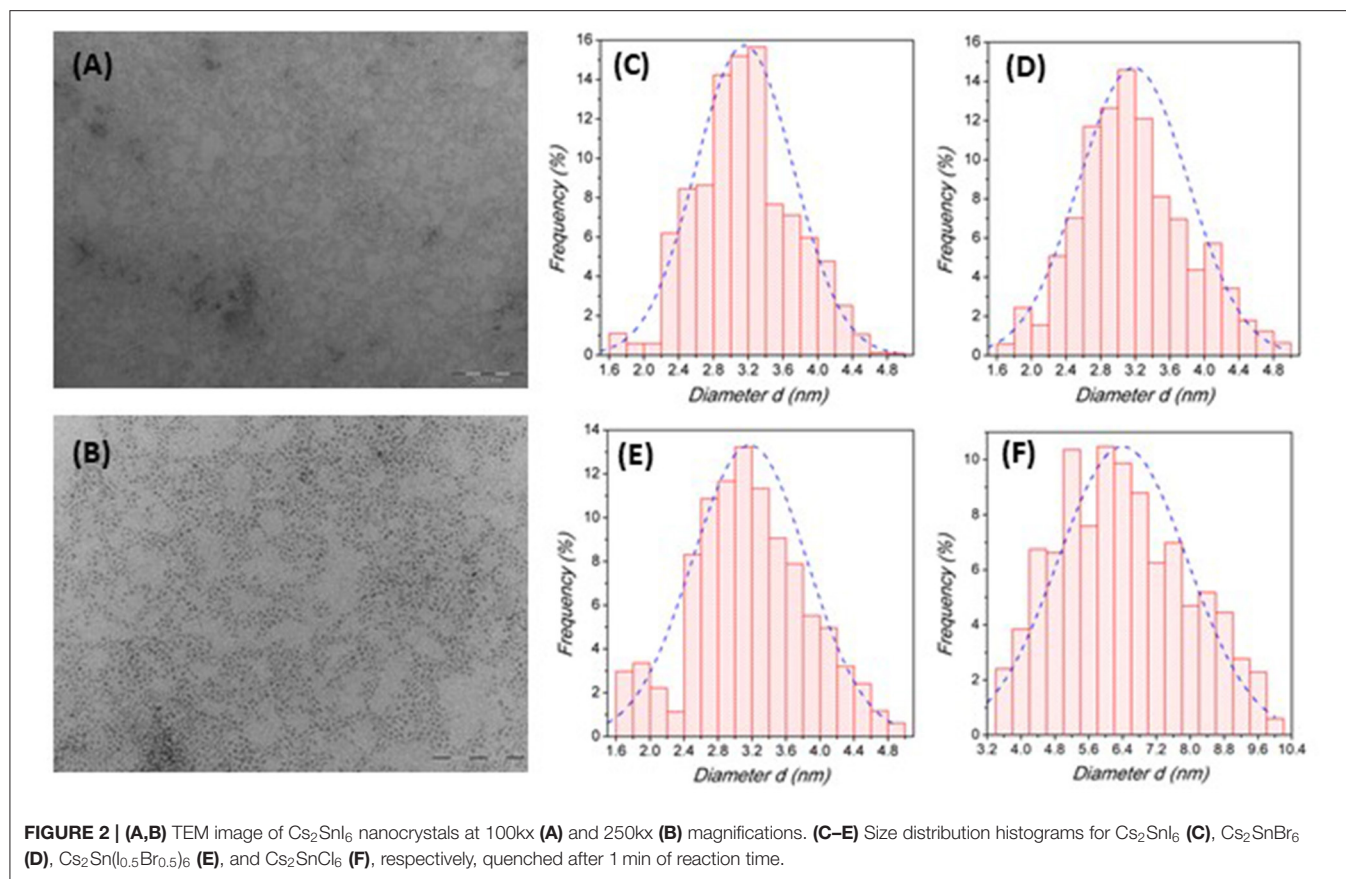
The transmission electron microscopy (TEM) investigation performed on the samples revealed the presence of spherical NCs with an average particle diameter,  $d$ , of about 3.2 nm for all the compositions of the  $\text{Cs}_2\text{SnX}_6$  system except for  $\text{Cs}_2\text{SnCl}_6$  nanocrystals which showed a greater particle size of about 6.4 nm. Such nanocrystal size is similar to that reported by Wang et al. and Ghosh et al. for  $\text{Cs}_2\text{SnI}_6$  and smaller than the recently reported data (Wang et al., 2016; Ghosh et al., 2018; Jing et al., 2019; Lin et al., 2019). **Figures 2A,B** report representative TEM images for the  $\text{Cs}_2\text{SnI}_6$  crystals at two magnifications (other TEM images in the **Supplementary Material**), while **Figures 2C–F** report the size distribution diagrams for the four compositions reacted for 1 min.

Overall, the size distribution for Br- and I-based samples is quite narrow and symmetric as for the mixed I/Br sample, while for  $\text{Cs}_2\text{SnCl}_6$  there is a clear evidence of a broader distribution. As reported in the Experimental Section, all these samples have been prepared by quenching the reaction after 1 min following the injection of the Cs-oleate precursor. We explored different quenching times (for the  $\text{Cs}_2\text{SnI}_6$  sample) by stopping the



reaction at 15 s, 1 min (data reported in **Figure 2C**), 2 and 10 min after precursor addition (size distribution diagrams and TEM images reported in the **Supplementary Material**). Again, the samples present a spherical shape with a size of about 2.9 nm for a reaction time of 15 s, and of about 3.2 nm for all the other times (data reported in the **Supplementary Material**). The results from TEM investigation on this series of samples (**Figure S3**) indicate that the formation of NCs is fast and occurs within few seconds after the precursor injection, while the crystal growth, on the contrary, is very slow and requires long times to produce significant variations in the particle diameter (no variation in the morphology—at least on the time-scale explored). The reduced growth rate can be attributed to the action of the ligands on the NC synthesis: it was observed, indeed, that using smaller amounts of capping agents resulted in spherical crystals with a diameter of 15–20 nm (Ghosh et al., 2018; Xu et al., 2019). This result is coherent with previous works on  $\text{Cs}_2\text{SnI}_6$  NCs reporting that

no NCs were obtained when oleic acid was the only capping agent used during the synthesis, thus suggesting a suppressing action of this ligand on the crystal growth (Wang et al., 2016). Dolzhenkov et al., instead, carried out their syntheses without using any organic ligand, and the samples prepared at 220°C were reported to have a diameter of about 38 nm (Dolzhenkov et al., 2017). A very recent work, on the other hand, made use of oleic acid only, without any amine, leading to  $\text{Cs}_2\text{SnI}_6$  NCs with an average size of 10–15 nm (Xu et al., 2019). It should be also noted that a narrow size distribution has been observed in most samples and for any reaction time, with standard deviations of 0.6 nm, except for the sample where the reaction has been stopped after 15 s (e.s.d. 1.2 nm), where a significantly broader size distribution has been observed. For stoichiometric samples,  $\text{Cs}_2\text{SnCl}_6$  shows, along with a bigger particle size, also a greater standard deviation with respect to I and Br containing NCs (**Figure 2F**). However, the general good focusing of particle size together with the slow



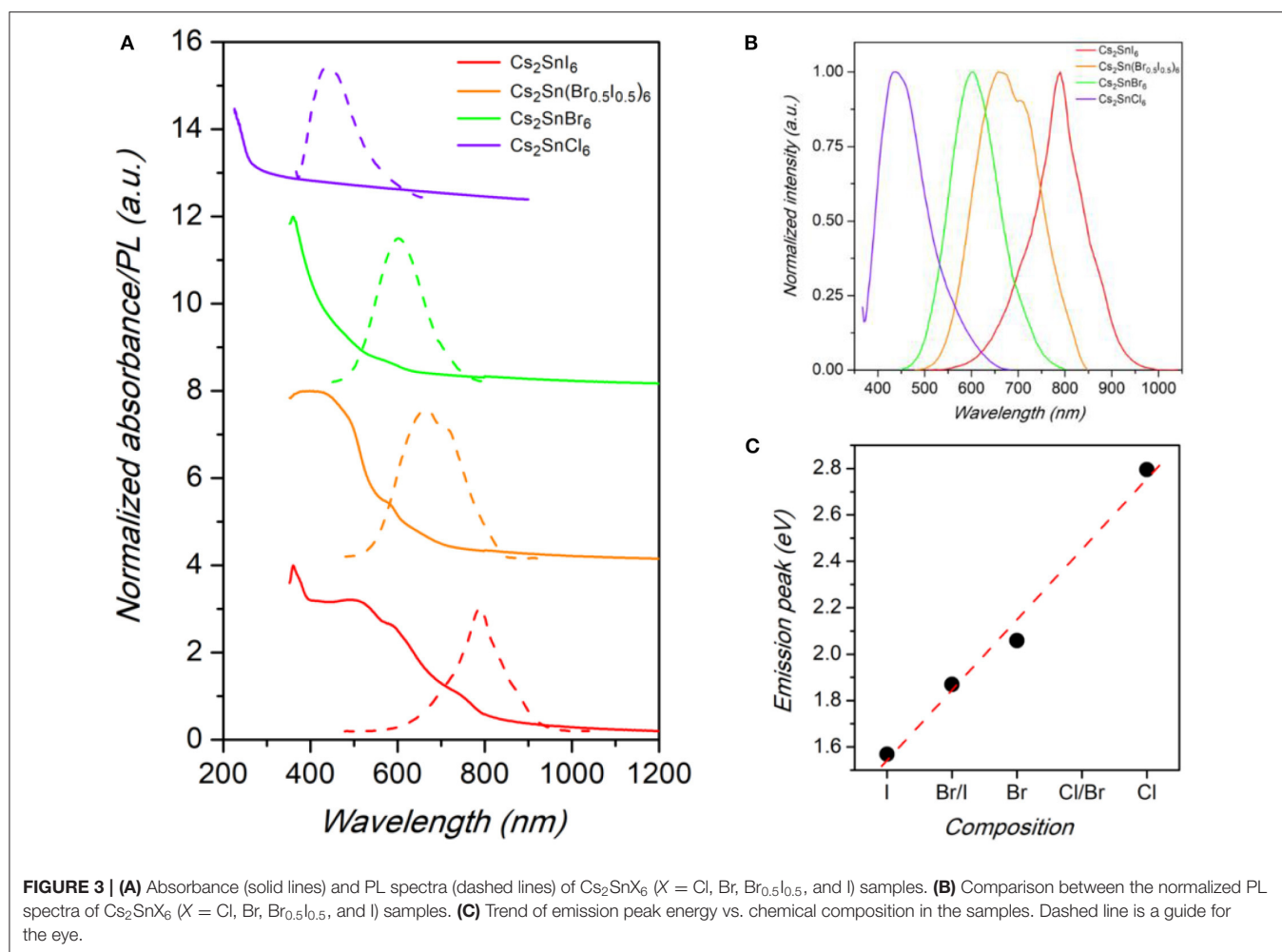
crystal growth can be very useful to achieve a good control over the NC size.

The optical properties of  $\text{Cs}_2\text{SnX}_6$  NCs were characterized by UV-vis-NIR absorbance and photoluminescence (PL) spectroscopy. Unlike lead halide NCs, that usually display a sharp absorption edge, the spectra were found to have a less distinct profile with a long tail pushing toward longer wavelengths (Figure 3A). In this regard, they are similar to the absorbance spectra of  $\text{CsSnX}_3$  NCs (Jellicoe et al., 2016). These results have been previously attributed to the presence of shallow electronic states, arising from crystal defects, such as halide vacancies, that have a low energy of formation and which are believed to introduce such states below the CB edge (Xiao et al., 2015; Maughan et al., 2016; Saparov et al., 2016).

The emission spectra of the  $\text{Cs}_2\text{SnX}_6$  NCs ( $X = \text{Cl}, \text{Br}, \text{Br}_{0.5}\text{I}_{0.5}, \text{I}$ ), reported in Figures 3A,B, are peaked at 444 nm (2.80 eV), 603 nm (2.06 eV), 663 nm (1.87 eV), and 790 nm (1.57 eV), by changing the halide content from Cl to I, with corresponding full-width at half maximum (FWHM) of 117, 122, 165, and 112 nm, respectively. The values we found for  $\text{Cs}_2\text{Sn}(\text{Br}_{0.5}\text{I}_{0.5})_6$  and  $\text{Cs}_2\text{SnI}_6$  NCs are considerably higher than the fundamental gap energies reported for these compounds in the bulk form (1.43 and 1.3 eV, respectively), thus suggesting a significant blue-shift in the NC optical properties due to quantum confinement effects (Kaltzoglou et al., 2015, 2016; Yuan et al., 2019). The values of the band gap extracted from the

Tauc plot of the absorbance spectra are reported in Table S1 of the Supplementary Material and confirms the scaling of the emission with a possible dependence of the Stoke shift with the halide nature. The trend of band gap of NCs compared to bulk samples is consistent with TEM investigation, that in fact revealed a very small diameter for the present crystals, and with previous studies on  $\text{Cs}_2\text{SnI}_6$  NCs (Wang et al., 2016; Dolzhenkov et al., 2017; Xu et al., 2019). In the case of  $\text{Cs}_2\text{SnBr}_6$  and  $\text{Cs}_2\text{SnCl}_6$ , instead, the PL peak energies are lower than the reported values of the bulk perovskites but in line with a linear scaling of the energy-gap variation with composition (see Figure 3C), thus suggesting a more significant impact of size reduction for these systems (Kaltzoglou et al., 2016). We highlight that the FWHM of the samples reported in this work, while larger with respect to state-of-the-art lead halide nanocrystals (typically 30–40 nm or even lower), are smaller than the values for the only published, to date, sample of the series investigated here, i.e.,  $\text{Cs}_2\text{SnI}_6$ , being of the order of 150–200 nm (Wang et al., 2016; Dolzhenkov et al., 2017; Xu et al., 2019).

Estimation of the quantum yield (QY) has been carried out as reported in the Experimental section. For all the NCs synthesized and characterized in the present work, the QYs range around 0.4–1.4%. Such values are quite low if compared to lead analogs, but improved with respect to the value of 0.48% reported for  $\text{Cs}_2\text{SnI}_6$  NCs by Wang et al. (2016).



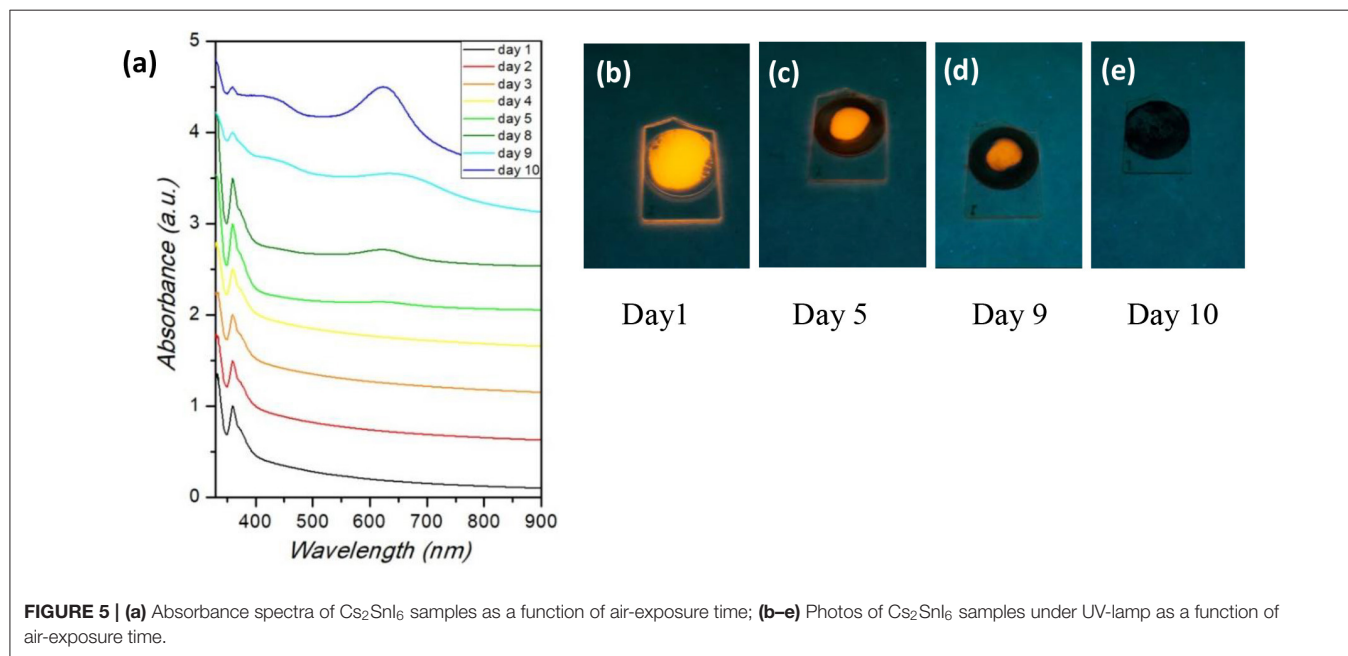
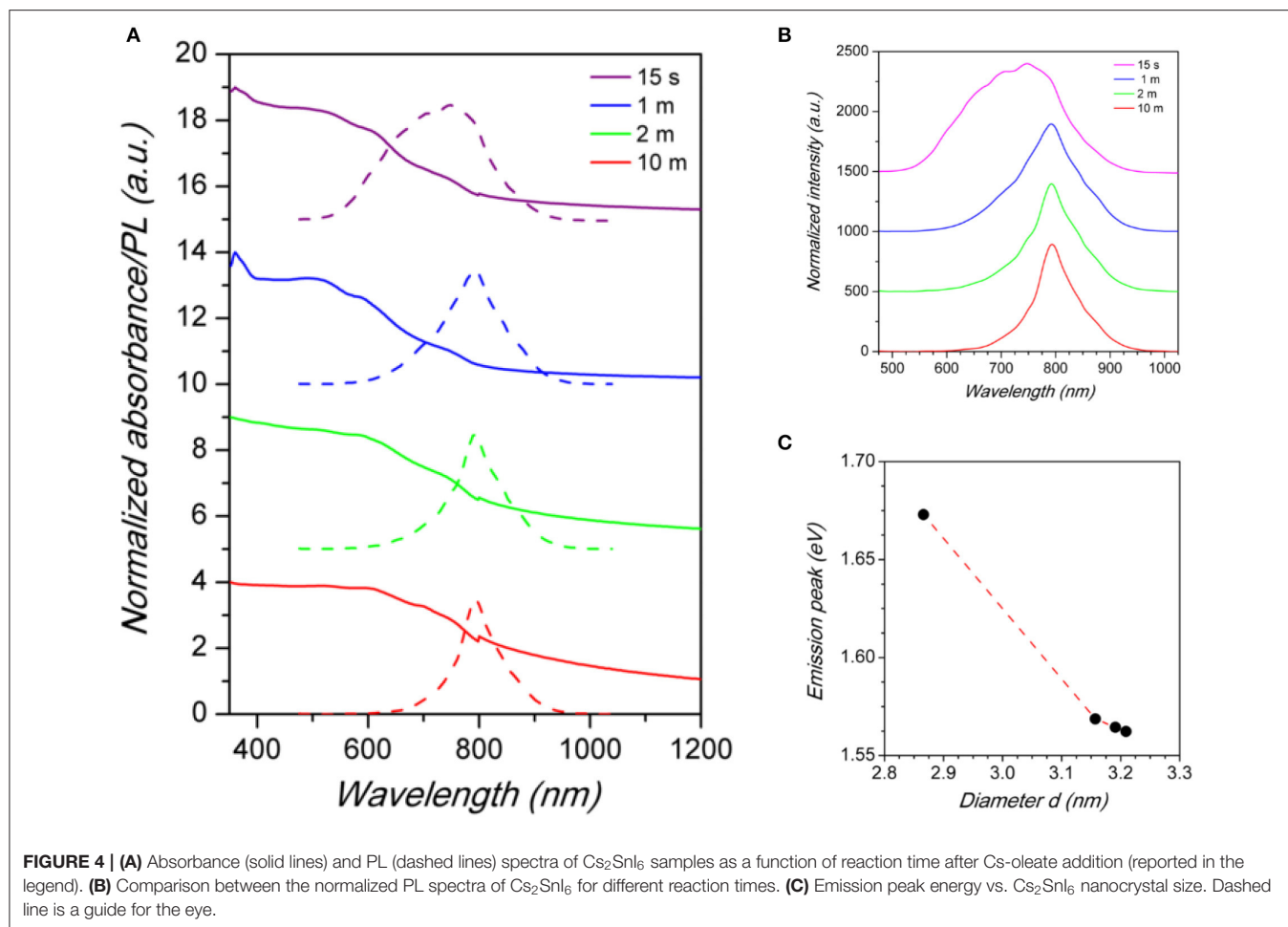
Absorption and emission optical measurements have been as well carried out on the  $\text{Cs}_2\text{SnI}_6$  series as a function of NCs reaction time discussed above (Figure 4A).

The PL spectra reported in Figure 4B reveal that the size of NCs has an impact on the luminescence properties of  $\text{Cs}_2\text{SnI}_6$ . By increasing the particle diameter from about 2.9 nm to about 3.2 (determined by TEM, see Supplementary Material), a red-shift of the emission peak is observed from about 741 nm (1.67 eV) to 793 nm (1.56 eV) (Figure 4C) which is a huge variation of the optical properties for a relatively small variation of the nanocrystal size. Moreover, crystal size affects as well the FWHM of PL spectra: the shift of the peak wavelength is indeed accompanied by a narrowing of the emission linewidth. As a matter of fact, the sample with the smallest NCs size presented the broadest peak of the series, with a FWHM of  $\sim 200$  nm, while, on the other hand, the sample reacted for 10 min has the narrowest one, with a FWHM of 79 nm (see the size distribution plots in the Supplementary Material). These results, due to quantum confinement effects arising from the small particle diameter, demonstrated that the luminescence properties of the  $\text{Cs}_2\text{SnX}_6$  NCs can be tuned, with the present synthetic protocol, by varying both their chemical composition and crystal size. Finally, and concerning air-stability, we highlight that the present

nanocrystals, deposited on a glass slide exposed to ambient conditions, retained their emission properties for about 10 days, thus already suggesting a good starting point to further enhance their stability by playing with the synthetic routes. This can be appreciated in Figures 5a–e reporting the absorbance as a function of time up to 10 days, as well as some selected photos at four time intervals (Day 1, 5, 9, and 10). Absorbance and UV-lamp photos (excitation at 365 nm) clearly show that up to 9 days of air exposure the spectra are unchanged and the red-emission is still evident. On the other hand, the spectra at Day 10 shows the appearance of a new profile peaked at about 600 nm deriving from decomposition products which is slightly observable already at Day 8, suggesting partial decomposition from this time.

## CONCLUSIONS

Nanocrystalline  $\text{Cs}_2\text{SnX}_6$  ( $X = \text{Cl}, \text{Br}, \text{Br}_{0.5}\text{I}_{0.5}, \text{I}$ ) samples have been prepared by a simple, optimized, hot-injection method without the use of toxic phosphines, reporting for the first time the synthesis of  $\text{Cs}_2\text{SnBr}_6$ , and mixed  $\text{Cs}_2\text{Sn}(\text{I}_{0.5}\text{Br}_{0.5})_6$  samples. The synthetic approach allowed to finely tune the anion composition and to prepare single-phase cubic samples with a



linear scaling of the unit cell volume along with the I/Br content. The prepared nanocrystals, for the same reaction time, have a spherical shape with average size in the range around 3–6 nm, depending on the composition. Optical properties have been nicely modulated by the halide content by progressively tuning the optical emission from ~440 nm for Cs<sub>2</sub>SnCl<sub>6</sub> to ~790 nm for Cs<sub>2</sub>SnI<sub>6</sub>, also showing that Sn<sup>4+</sup>-based perovskites-derivatives have a lower energy gap, when compared to their lead-based counterpart, reaching the NIR region; this contributes to make them potentially better materials for photovoltaic applications and widen the optical range of this class of known materials. In addition, the prepared samples showed stable emission properties under ambient conditions for several days. By varying the reaction time from 15 s to 10 min the nanocrystal size showed only a limited growth (from about 2.9–3.2 nm) which however resulted in a progressive red-shift of about 0.1 eV of the band gap as well as in a reduction of the PL spectra FWHM from 210 to about 80 nm. The present results add a significant contribution toward the discovery of new lead-free nanocrystalline phases with enhanced air-stability by showing, for the first time, an easy and reliable tuning of optical properties of perovskite-derivatives by anion composition in analogy with the results available for 3D lead halide perovskites.

## EXPERIMENTAL SECTION

### Chemicals

Cs<sub>2</sub>CO<sub>3</sub> (Acros Organics, 99.995%), SnCl<sub>4</sub> (Sigma-Aldrich, 99.995%), SnBr<sub>4</sub> (Sigma-Aldrich, 99%), SnI<sub>4</sub> (Sigma-Aldrich, 99.999%), 1-octadecene (ODE, Acros Organics, 90%), oleic acid (OA, VWR Chemicals, 81%), oleylamine (OLA, Acros Organics, 80–90%), hexane (HEX, Sigma-Aldrich ≥99%), 1-butanol (BUT, Sigma-Aldrich, ≥99.4%). All reagents were used without further purification.

### Synthesis

#### Synthesis of Cs-Oleate

Fifteen milliliters of ODE was loaded in a 50 mL three-neck flask along with 0.5 mL of OA and 0.5 mL of OLA and dried under vacuum for 1 h at 120°C. After that, 0.1625 g of Cs<sub>2</sub>CO<sub>3</sub> was added to the reaction vessel and the mixture was dried again under vacuum for 1 h at the same temperature. Finally, the flask was heated at 150°C under nitrogen flow until complete dissolution of Cs<sub>2</sub>CO<sub>3</sub>. The resulting solution was stored under nitrogen atmosphere. Since Cs-oleate is insoluble in ODE at room temperature, we preheated the solution at 130°C to dissolve the precipitate before use.

#### Synthesis of Cs<sub>2</sub>SnX<sub>6</sub> NCs

ODE (5 mL), OA (0.2 mL), and OLA (0.2 mL) were combined in a 50 mL three-neck flask and dried under vacuum for 1 h at 120°C. Subsequently, 0.235 mmol of SnX<sub>4</sub> (0.1468 g of SnI<sub>4</sub>, 0.1027 g of SnBr<sub>4</sub>, and 0.0611 g of SnCl<sub>4</sub>, respectively) was added to the flask and the solution was degassed under vacuum for 15 min at 80°C. In the case of mixed-composition NCs, an equimolar ratio of SnBr<sub>4</sub> and SnI<sub>4</sub> was used. The flask was then heated at 220°C under nitrogen flow and 1.5 mL of

the as-prepared Cs-oleate solution was quickly injected with vigorous stirring. After a specific reaction time (15 s, 1 min, 2 min, 10 min), the mixture was cooled down in an ice bath. To purify the NCs, the mother solution was centrifuged at 7,000 rpm for 5 min and the surfactant was discarded. Some of the crystals were deposited on glass slides and covered with cover-slips, while the remaining crystals were dispersed in 5 mL of HEX. No argon-filled glovebox was needed during the synthesis and the purification process, nor to store the final samples. The stoichiometry of the samples was checked with Energy Dispersive X-ray (EDX) spectroscopy and was found to be in agreement with the nominal one within an e.s.d. of 5%.

### TEM

Transmission electron microscopy (TEM) was performed on a JEOL JEM-1200 EX II microscope operating at 100 kV, equipped with a tungsten filament as electron source. The specimens were prepared by depositing 8 μL of NCs in HEX on an aluminum grid covered with a polymeric film and letting the solvent evaporate under ambient condition. The size distribution of the samples was calculated from TEM images using ImageJ software.

### XRD

X-ray diffraction (XRD) investigations were carried out under ambient condition on a Bruker D8 Advance diffractometer using copper K $\alpha$  radiation ( $\lambda = 1.54056 \text{ \AA}$ ) as X-ray source. The measurements were performed in the Bragg-Brentano configuration, with resolution of 0.04° and integration time of 4 sec. The specimens were prepared by depositing the NCs on a glass slide and covering them with a glass cover slip. The reference patterns and crystal constants were calculated using PowderCell software. Lattice parameters were determined from Rietveld refinement of the diffraction pattern.

### Absorption Spectroscopy

Ultraviolet-Visible-Near Infrared (UV-Vis-NIR) absorption measurements were performed under ambient conditions using a Varian Cary 6000i spectrophotometer equipped with a double monochromator, a deuterium lamp and a tungsten filament lamp as light sources, a photomultiplier (UV-Vis) and an InGaAs photodiode (NIR) as detectors. Spectral range was 200–1,800 nm, in step of 2 nm. The specimens were prepared by depositing the NCs on a glass slide and covering them with a glass cover slip. The baseline was taken using the glass slide as reference.

### Steady-State PL Spectroscopy

PL investigations were conducted under ambient conditions using a 355 nm laser line (PowerChip Microlaser) as excitation light source and a LN<sub>2</sub>-cooled silicon CCD (Princeton Instruments Spec-10:400) as detector. The specimens were prepared by depositing the NCs on a glass slide and covering them with a glass cover slip. Measurements were performed in transmission mode, with a resolution of 0.5 nm and an

integration time of 5 sec, using a longpass filter at 450 nm to remove the laser line from the PL signal. The background noise and the luminescence from the glass slide were subtracted from the spectra of the samples. Since PL signals were not perfectly symmetric Gaussian curves, the emission peak positions were determined by fitting the spectra a Gaussian lineshape.

## Photoluminescence Quantum Yield

PL QY measurements were performed on the samples dispersed in HEX into quartz cuvettes (1 cm optical path) using a Varian Cary Eclipse Fluorescence Spectrophotometer with an excitation wavelength of 350 nm. We used Rhodamine B and Rhodamine 6G in ethanol as standards to calculate the QY values for the NCs.

## Energy Dispersive X-Ray Spectroscopy

Energy dispersive x-ray spectroscopy (EDX) has been performed with a high-resolution scanning electron microscope (SEM, TESCAN Mira 3) operated at 15 kV. For all the samples it was found an experimental cation/anion ratio in agreement (within a 5% error) with the nominal compositions. Also for mixed Br/I compositions the anion ration expected by the stoichiometry was confirmed experimentally.

## REFERENCES

- Amgar, D., Aharon, S., and Etgar, L. (2016). Inorganic and hybrid organo-metal perovskite nanostructures: synthesis, properties, and applications. *Adv. Funct. Mater.* 26, 8576–8593. doi: 10.1002/adfm.201603752
- Bekenstein, Y., Dahl, J. C., Huang, J., Osowiecki, W. T., Swabeck, J. K., Chan, E. M., et al. (2018). The making and breaking of lead-free double perovskite nanocrystals of cesium silver-bismuth halide compositions. *Nano Lett.* 18, 3502–3508. doi: 10.1021/acs.nanolett.8b00560
- Cai, Y., Xie, W., Ding, H., Chen, Y., Thirumal, K., Wong, L. H., et al. (2017). Computational study of halide perovskite-derived  $A_2BX_6$  inorganic compounds: chemical trends in electronic structure and structural stability. *Chem. Mater.* 29, 7740–7749. doi: 10.1021/acs.chemmater.7b02013
- Creutz, S. E., Crites, E. N., De Siena, M. C., and Gamelin, D. R. (2018). Colloidal nanocrystals of lead-free double-perovskite (elpasolite) semiconductors: synthesis and anion exchange to access new materials. *Nano Lett.* 18, 1118–1123. doi: 10.1021/acs.nanolett.7b04659
- Dalpian, G. M., Liu, Q., Stoumpos, C. C., Douvalis, A. P., Balasubramanian, M., Kanatzidis, M. G., et al. (2017). Changes in charge density vs changes in formal oxidation states: the case of Sn halide perovskites and their ordered vacancy analogues. *Phys. Rev. Mater.* 1:025401. doi: 10.1103/PhysRevMaterials.1.025401
- Dolzhnikov, D. S., Wang, C., Xu, Y., Kanatzidis, M. G., and Weiss, E. A. (2017). Ligand-free, quantum-confined  $Cs_2SnI_6$  perovskite nanocrystals. *Chem. Mater.* 29, 7901–7907. doi: 10.1021/acs.chemmater.7b02803
- Ferrara, C., Patrini, M., Pisanu, A., Quadrelli, P., Milanese, C., Tealdi, C., et al. (2017). Wide band-gap tuning in Sn-based hybrid perovskites through cation replacement: the  $FA_{1-x}MA_xSnBr_3$  mixed system. *J. Mater. Chem. A* 5, 9391–9395. doi: 10.1039/C7TA01668A
- Ghosh, S., Paul, S., and De, S. K. (2018). Control synthesis of air-stable morphology tunable Pb-free  $Cs_2SnI_6$  perovskite nanoparticles and their photodetection properties. *Part. Part. Syst. Charact.* 35:1800199. doi: 10.1002/ppsc.201800199
- Hermann, A., Furthmüller, J., Gäggeler, H. W., and Schwerdtfeger, P. (2010). Spin-orbit effects in structural and electronic properties for the solid state of the group-14 elements from carbon to superheavy element 114. *Phys. Rev. B* 82:155116. doi: 10.1103/PhysRevB.82.155116

## DATA AVAILABILITY STATEMENT

All datasets generated for this study are included in the article/**Supplementary Material**.

## AUTHOR CONTRIBUTIONS

AV and CC carried out synthesis and PL measurements. MP supervised the optical measurements and coordinated the work. PQ supervised the material synthesis. DB contributed to spectroscopic measurements. LM devised the work and coordinated the whole activity. LM and MP wrote the manuscript.

## ACKNOWLEDGMENTS

The authors gratefully acknowledge the Centro Grandi Strumenti (CGS) of University of Pavia for TEM measurements.

## SUPPLEMENTARY MATERIAL

The Supplementary Material for this article can be found online at: <https://www.frontiersin.org/articles/10.3389/fchem.2020.00035/full#supplementary-material>

- Huang, H., Bodnarchuk, M. I., Kershaw, S. V., Kovalenko, M. V., and Rogach, A. L. (2017). Lead halide perovskite nanocrystals in the research spotlight: stability and defect tolerance. *ACS Energy Lett.* 2, 2071–2083. doi: 10.1021/acsenergylett.7b00547
- Huang, H., Polavarapu, L., Sichert, J. A., Susa, A. S., Urban, A. S., and Rogach, A. L. (2016). Colloidal lead halide perovskite nanocrystals: synthesis, optical properties and applications. *NPG Asia Mater.* 8:e328. doi: 10.1038/am.2016.167
- Jellicoe, T. C., Richter, J. M., Glass, H. F. J., Tabachnyk, M., Brady, R., Dutton, S. E., et al. (2016). Synthesis and optical properties of lead-free cesium tin halide perovskite nanocrystals. *J. Am. Chem. Soc.* 138, 2941–2944. doi: 10.1021/jacs.5b13470
- Jing, Y., Liu, Y., Zhao, J., and Xia, Z. (2019). Sb<sup>3+</sup> Doping-induced triplet self-trapped excitons emission in lead-free  $Cs_2SnCl_6$  nanocrystals. *J. Phys. Chem. Lett.* 10, 7439–7444. doi: 10.1021/acs.jpcclett.9b03035
- Ju, M.-G., Chen, M., Zhou, Y., Garces, H. F., Dai, J., Ma, L., et al. (2018). Earth-abundant nontoxic titanium(IV)-based vacancy-ordered double perovskite halides with tunable 1.0 to 1.8 eV bandgaps for photovoltaic applications. *ACS Energy Lett.* 3, 297–304. doi: 10.1021/acsenergylett.7b01167
- Kaltzoglou, A., Antoniadou, M., Kontos, A. G., Stoumpos, C. C., Perganti, D., Siranidi, E., et al. (2016). Optical-vibrational properties of the  $Cs_2SnX_6$  (X = Cl, Br, I) defect perovskites and hole-transport efficiency in dye-sensitized solar cells. *J. Phys. Chem. C* 120, 11777–11785. doi: 10.1021/acs.jpcc.6b02175
- Kaltzoglou, A., Antoniadou, M., Perganti, D., Siranidi, E., Raptis, V., Trohidou, K., et al. (2015). Mixed-halide  $Cs_2SnI_3Br_3$  perovskite as low resistance hole-transporting material in dye-sensitized solar cells. *Electrochim. Acta* 184, 466–474. doi: 10.1016/j.electacta.2015.10.030
- Kovalenko, M. V., Protesescu, L., and Bodnarchuk, M. I. (2017). Properties and potential optoelectronic applications of lead halide perovskite nanocrystals. *Science* 358, 745–750. doi: 10.1126/science.aam7093
- Leng, M., Yang, Y., Zeng, K., Chen, Z., Tan, Z., Li, S., et al. (2018). All-inorganic bismuth-based perovskite quantum dots with bright blue photoluminescence and excellent stability. *Adv. Funct. Mater.* 28:1704446. doi: 10.1002/adfm.201704446
- Lin, T.-W., Su, C., and Lin, C. C. (2019). Phase transition and energy transfer of lead-free  $Cs_2SnCl_6$  perovskite nanocrystals by controlling

- the precursors and doping manganese ions. *J. Inf. Disp.* 20, 209–216. doi: 10.1080/15980316.2019.1655493
- Liu, F., Ding, C., Zhang, Y., Ripolles, T. S., Kamisaka, T., Toyoda, T., et al. (2017). Colloidal synthesis of air-stable alloyed  $\text{CsSn}_{1-x}\text{Pb}_x\text{I}_3$  perovskite nanocrystals for use in solar cells. *J. Am. Chem. Soc.* 139, 16708–16719. doi: 10.1021/jacs.7b08628
- Mancini, A., Quadrelli, P., Milanese, C., Patrini, M., Guizzetti, G., and Malavasi, L. (2015).  $\text{CH}_3\text{NH}_3\text{Sn}_x\text{Pb}_{1-x}\text{Br}_3$  Hybrid perovskite solid solution: synthesis, structure, and optical properties. *Inorg. Chem.* 54, 8893–8895. doi: 10.1021/acs.inorgchem.5b01843
- Maughan, A. E., Ganose, A. M., Bordelon, M. M., Miller, E. M., Scanlon, D. O., and Neilson, J. R. (2016). Defect tolerance to intolerance in the vacancy-ordered double perovskite semiconductors  $\text{Cs}_2\text{SnI}_6$  and  $\text{Cs}_2\text{TeI}_6$ . *J. Am. Chem. Soc.* 138, 8453–8464. doi: 10.1021/jacs.6b03207
- Pal, J., Manna, S., Mondal, A., Das, S., Adarsh, K. V., and Nag, A. (2017). Colloidal synthesis and photophysics of  $\text{M}_3\text{Sb}_2\text{I}_9$  ( $\text{M}=\text{Cs}$  and  $\text{Rb}$ ) nanocrystals: lead-free perovskites. *Angew. Chem.* 129, 14375–14379. doi: 10.1002/ange.201709040
- Pisanu, A., Mahata, A., Mosconi, E., Patrini, M., Quadrelli, P., Milanese, C., et al. (2018). Exploring the limits of three-dimensional perovskites: the case of  $\text{FAPb}_{1-x}\text{Sn}_x\text{Br}_3$ . *ACS Energy Lett.* 3, 1353–1359. doi: 10.1021/acsenergylett.8b00615
- Saparov, B., Sun, J.-P., Meng, W., Xiao, Z., Duan, H.-S., Gunawan, O., et al. (2016). Thin-film deposition and characterization of a Sn-deficient perovskite derivative  $\text{Cs}_2\text{SnI}_6$ . *Chem. Mater.* 28, 2315–2322. doi: 10.1021/acs.chemmater.6b00433
- Sun, J., Yang, J., Lee, J. I., Cho, J. H., and Kang, M. S. (2018). Lead-free perovskite nanocrystals for light-emitting devices. *J. Phys. Chem. Lett.* 9, 1573–1583. doi: 10.1021/acs.jpcclett.8b00301
- Swarnkar, A., Ravi, V. K., and Nag, A. (2017). Beyond colloidal cesium lead halide perovskite nanocrystals: analogous metal halides and doping. *ACS Energy Lett.* 2, 1089–1098. doi: 10.1021/acsenergylett.7b00191
- Umari, P., Mosconi, E., and De Angelis, F. (2015). Relativistic GW calculations on  $\text{CH}_3\text{NH}_3\text{PbI}_3$  and  $\text{CH}_3\text{NH}_3\text{SnI}_3$  perovskites for solar cell applications. *Sci. Rep.* 4:4467. doi: 10.1038/srep04467
- Wang, A., Guo, Y., Muhammad, F., and Deng, Z. (2017). Controlled synthesis of lead-free cesium tin halide perovskite cubic nanocages with high stability. *Chem. Mater.* 29, 6493–6501. doi: 10.1021/acs.chemmater.7b02089
- Wang, A., Yan, X., Zhang, M., Sun, S., Yang, M., Shen, W., et al. (2016). Controlled synthesis of lead-free and stable perovskite derivative  $\text{Cs}_2\text{SnI}_6$  nanocrystals via a facile hot-injection process. *Chem. Mater.* 28, 8132–8140. doi: 10.1021/acs.chemmater.6b01329
- Wu, X., Song, W., Li, Q., Zhao, X., He, D., and Quan, Z. (2018). Synthesis of lead-free  $\text{CsGeI}_3$  perovskite colloidal nanocrystals and electron beam-induced transformations. *Chem. An Asian J.* 13, 1654–1659. doi: 10.1002/asia.201800573
- Xiao, Z., Zhou, Y., Hosono, H., and Kamiya, T. (2015). Intrinsic defects in a photovoltaic perovskite variant  $\text{Cs}_2\text{SnI}_6$ . *Phys. Chem. Chem. Phys.* 17, 18900–18903. doi: 10.1039/C5CP03102H
- Xu, Y., Li, S., Zhang, Z., Hu, Y., Yuan, L., Chen, W., et al. (2019). Ligand-mediated synthesis of colloidal  $\text{Cs}_2\text{SnI}_6$  three-dimensional nanocrystals and two-dimensional nanoplatelets. *Nanotechnology* 30:295601. doi: 10.1088/1361-6528/ab13f6
- Yang, B., Chen, J., Hong, F., Mao, X., Zheng, K., Yang, S., et al. (2017). Lead-free, air-stable all-inorganic cesium bismuth halide perovskite nanocrystals. *Angew. Chem.* 129, 12645–12649. doi: 10.1002/ange.201704739
- Yuan, G., Huang, S., Qin, S., Wu, X., Ding, H., and Lu, A. (2019). Structural, optical, and thermal properties of  $\text{Cs}_2\text{SnI}_{6-x}\text{Br}_x$  mixed perovskite solid solutions. *Eur. J. Inorg. Chem.* 2019, 2524–2529. doi: 10.1002/ejic.201900120
- Zhang, J., Yang, Y., Deng, H., Farooq, U., Yang, X., Khan, J., et al. (2017). High quantum yield blue emission from lead-free inorganic antimony halide perovskite colloidal quantum dots. *ACS Nano* 11, 9294–9302. doi: 10.1021/acsnano.7b04683
- Zhou, L., Liao, J.-F., Huang, Z.-G., Wang, X.-D., Xu, Y.-F., Chen, H.-Y., et al. (2018a). All-inorganic lead-free  $\text{Cs}_2\text{PdX}_6$  ( $\text{X}=\text{Br}, \text{I}$ ) perovskite nanocrystals with single unit cell thickness and high stability. *ACS Energy Lett.* 3, 2613–2619. doi: 10.1021/acsenergylett.8b01770
- Zhou, L., Xu, Y.-F., Chen, B.-X., Kuang, D.-B., and Su, C.-Y. (2018b). Synthesis and photocatalytic application of stable lead-free  $\text{Cs}_2\text{AgBiBr}_6$  perovskite nanocrystals. *Small* 14:1703762. doi: 10.1002/sml.201703762

**Conflict of Interest:** The authors declare that the research was conducted in the absence of any commercial or financial relationships that could be construed as a potential conflict of interest.

Copyright © 2020 Veronese, Patrini, Bajoni, Ciarrocchi, Quadrelli and Malavasi. This is an open-access article distributed under the terms of the Creative Commons Attribution License (CC BY). The use, distribution or reproduction in other forums is permitted, provided the original author(s) and the copyright owner(s) are credited and that the original publication in this journal is cited, in accordance with accepted academic practice. No use, distribution or reproduction is permitted which does not comply with these terms.